Springer

KSME

Journal of Mechanical Science and Technology 29 (4) (2015) 1765~1779
www.springerlink.com/content/1738-494x
DOI 10.1007/s12206-015-0350-4

Thermal performance assessment in a fin-and-oval-tube heat exchanger with delta winglet vortex generators †

Withada Jedsadaratanachai[1,*] and Amnart Boonloi[2]

[1]*Department of Mechanical Engineering, Faculty of Engineering, King Mongkut's Institute of Technology Ladkrabang, Bangkok 10520, Thailand*
[2]*Department of Mechanical Engineering Technology, College of Industrial Technology, King Mongkut's University of Technology North Bangkok, Bangkok 10800, Thailand*

(Manuscript Received July 31, 2014; Revised December 10, 2014; Accepted December 21, 2014)

Abstract

Thermal performance assessments, flow configurations and heat transfer characteristics in a fin-and-oval-tube heat exchanger with the delta winglet vortex generators are examined numerically. Delta winglet vortex generators like V-ribs are placed on fin surfaces with V-tip pointing upstream called "V-Upstream". The effects of the flow attack angles (α = 15°, 30°, 45° and 60°) and the distances between V-tip to the center of the oval tube in transverse line (Transverse pitch, a = 3.77, 4.77 and 5.77 mm) on heat transfer, flow structure and thermal performance are studied for Reynolds number based on the hydraulic diameter of the test channel, Re = 500 - 2500. The numerical results are presented in four parts: validations of the base case, flow configurations, velocity field, heat transfer and thermal performance assessment. It is found that the use of the delta winglet vortex generators can help to improve heat transfer rate in the heating system by creating vortex flow and swirl flow over the test channel. The heat transfer and pressure loss appeared to be higher than the plain fin for all case studies. The augmentation of the flow attack angle results in the rise of heat transfer rate and friction loss, while differences in transverse pitch produced similar values in terms of the Nusselt number and friction loss. In addition, augmentations are found around 1.15 - 1.55 and 1.5 - 3.4 times over the base case for heat transfer and friction factor, respectively. At Re = 2500, a = 5.77 mm and α = 15°, the maximum thermal enhancement factor is found to be around 1.12.

Keywords: Fin-and-oval-tube; Flow configuration; Heat exchanger; Heat transfer characteristic; V-Upstream

1. Introduction

Vortex generators or turbulators, such as wing, winglet, rib, baffle, and groove, are used in various types of heat exchanger to improve heat transfer rate and thermal performance. The improvements of heat system are done by changing the fluid flow structure and inducing vortex flow or swirl flow over the heating system. The fin-and-tube heat exchanger is one type of heat exchanger used in many industries: chemical, automotive, air conditioning, refrigeration, electronic equipment, etc. Vortex generators are also applied to the fin-and-tube heat exchanger due to the compact size is needed, especially for electronic equipment.

Many investigators have presented the use of V-shaped turbulators to enhance the thermal performance in a square channel, rectangular channel and circular tube. Pauley and Eaton [1] investigated the effects of the spacing between the edges of vortex generators (2 - 14 cm) and flow attack angles (6° - 24°) on flow structure and heat transfer behavior. They reported that the enhancement of the Stanton number varied in the range 8 - 30%, depending on the vortex strength created from the vortex generators. Wroblewski and Eibeck [2] studied delta winglet vortex generators on thermal performance and found that the optimum thermal performance was around 25% at the flow attack angle of 12°. The difference of the common–flow–up and common–flow–down for delta winglet vortex generators in a rectangular channel was presented by Kim and Yang [3]. They concluded that the common-flow-down performs better in terms of heat transfer than the common-flow-up at similar conditions. The thermal performance assessments on ten pairs of rectangular winglet vortex generators placed on the entrance regime in a solar air heater channel were reported by Depaiwa et al. [4]. The influences of flow attack angles (α = 30° - 60°) and arrangements (V–tip pointing upstream called "V–Upstream" and V–tip pointing downstream called "V–Downstream") were studied for Reynolds number based on the hydraulic diameter of the rectangular channel, Re = 5000 - 23000. They summarized that the increasing the flow attack angle performs the highest on both heat transfer and friction factor. They also claimed that the

*Corresponding author. Tel.: +662 3298350, Fax.: +662 3298352
E-mail address: kjwithad@kmitl.ac.th
† Recommended by Associate Editor Ji Hwan Jeong

rectangular winglet vortex generators with V–Downstream case provide higher heat transfer rate than the V–Upstream case. The effects of longitudinal vortex generators placed in a horizontal narrow rectangular channel on heat transfer and friction loss were studied by Qiuwang et al. [5]. They reported that the augmentation of heat transfer is around 10 - 45% and also concluded that longitudinal vortex generators placed on both two sides of the channel give a higher thermal performance than only one side of the channel. The investigations of four pair longitudinal vortex generators on heat transfer and friction loss on both laminar and turbulent regimes were reported by Jian et al. [6]. They found that the heat transfer is increasing around 100.9% and 87.1%, respectively, for laminar and turbulent regimes, while the pressure loss is around 11.4% and 100.3% for laminar and turbulent, respectively. Min et al. [7] investigated heat transfer characteristics in a channel with rectangular winglet vortex generators for turbulent regime, Re = 5000 - 17500. They found that the heat transfer rate increased around 46 - 55%. The numerical investigations on various type vortex generators in a circular tube were reported by Charbel et al. [8]. They concluded that the augmentation on heat transfer is due to the better mixing of the fluid flow and also the presence of the vortex flow near the heated wall of the test channel. Sarac and Bali [9] studied swirling flow on heat transfer and pressure loss in a horizontal pipe at Re = 5000 - 30000. They found that the increase in the Nusselt number was around 18.1 - 163% depending on Reynolds number, position of the vortex generators and flow attack angle. They also summarized that the increase of the flow attack angle leads to the rise of the Nusselt number. The influences of rectangular winglet vortex generators placed on the lower wall of a channel on thermal performance for Re = 800 - 3000 were investigated by Wu and Tao [10, 11]. They claimed that the rise of the flow attack angle is a key to increase in heat transfer rates over the test channel. Biswas and Chattopadhyay [12] numerically investigated the thermal performance of delta wing vortex generators in a rectangular channel. They reported that the augmentation on heat transfer was around 45.4% higher than the smooth channel for the flow attack angle of 20^o. Ahmed et al. [13] studied various types of vortex generators in a rectangular channel on both laminar and turbulent regimes. Their results showed that the delta wing can create counter-rotating flow over the test channel. Hiravennavar et al. [14] examined delta winglet vortex generators in the hydro–dynamically developed and thermally developing laminar rectangular channel flow. The results revealed that the enhancements were around 33% and 67% for single winglet and winglet pairs, respectively, when compared with the smooth channel. The thermal performance evaluations for the laminar region in a rectangular channel with delta–wings and delta–winglet pair vortex generators were examined by Biswas et al. [15]. They found that the delta–wing vortex generators are more effective than the winglet–pair, but the use of winglets appears to be a more attractive augmentation technique. Sohankar [16] studied the heat transfer characteristics in a rectangular channel with different flow attack angles of rib (10^o - 30^o) for Re = 200 - 2000. They found that the heat transfer performs steadily at lower Reynolds number, while it becomes unsteady at high Reynolds number values.

The use of vortex generators in fin–and–tube compact heat exchanger had been studied. Leu et al. [17] studied both numerically and experimentally the heat transfer characteristics and flow configurations in a fin–and–tube heat exchanger with inclined vortex generators placed behind the tube. They claimed inclined vortex generators can help to create the longitudinal vortex flow that leads to the increase in heat transfer rate and thermal performance over the plain fin. Sommers and Jacobi [18] studied experimentally for a refrigerator evaporator on the air–side with vortex generators. Their results revealed that the vortex generators can decrease the thermal resistance around 35 - 42% for Reynolds number 500 - 1300. Pesteei et al. [19] studied the effects of winglet positions on heat transfer and pressure loss. They found that the location in the downstream side case is the most effective to enhance the heat transfer rate. The investigations on heat transfer increases in a finned–oval–tube with inline longitudinal vortex generators [20] and with staggered longitudinal vortex generators [21] have been reported. Tiwari et al. [22] numerically studied the effects of delta winglet vortex generators in a fin–and–oval–tube for laminar flow. The numerical results showed that the use of the delta winglet vortex generators helps to increase heat transfer rates over the base case. O'Brien et al. [23] investigated heat transfer and flow structure in a narrow rectangular channel elliptical tube with one or two delta–winglet pairs. They summarized that the use of the winglet leads to an increase in heat transfer rate around 38% over the base case. Chu et al. [24] studied heat transfer characteristics and fluid flow structure of a fin–and–oval–tube heat exchangers with longitudinal vortex generators. The enhancements were around 13.6-32.9% and 29.2-40.6% when compared with the baseline case for heat transfer and friction loss, respectively. ElSherbini and Jacobi [25] presented an experimental investigation on heat transfer and friction factor in a fin–and–tube heat exchanger with delta winglet vortex generators for Re = 700 - 2300. They concluded that the Colburn j factor is around 31% in comparison with the baseline case. Joardar and Jacobi [26] studied the use of winglet type vortex generators in a compact plain–fin–and–tube heat exchanger on heat transfer enhancement and pressure loss. They found that the air–side heat transfer augmentations were around 16.5 - 44% and 29.9 - 69.8% for the single row and three row winglet arrangements at Re = 220 - 960, respectively. Joardar and Jacobi [27] also reported the effect of the three types winglet array: single-VG pair, 3VG-inline array and 3VG-staggered, on heat transfer and flow configuration at Re = 330 - 850. They summarized that the impinging flow on the tube wall is a reason for heat transfer augmentation. Kwak et al. [28] reported that triangular winglets placed in a fin-tube heat exchanger with in-line arrangement give higher heat transfer rate and pressure

loss around 10 - 25% and 20 - 35%, respectively, for Re = 300 - 2700. Russell et al. [29] investigated the heat transfer and friction loss in a plate-fin-and-tube heat exchanger with vortex generators and found that the ratio between Colburn-j factor and friction factor is more than 0.5.

According to above literature reviews, the use of V–shaped generators is more effective than other shapes, especially V–Downstream arrangement. However, the application of V-shaped generators in a fin–and–oval tube compact heat exchanger may be given to very large pressure losses, due to the small space between the fins. Therefore, the V–Upstream vortex generators, which help to reduce the pressure loss over the heating system, remain the flow configuration of primary interest. In the current work, numerical investigations are performed on flow configurations, heat transfer behaviors and thermal performance assessments in the fin–and–oval–tube compact heat exchanger with V–Upstream delta winglet vortex generators. The system is set as a channel heat exchanger [30]; the delta winglet vortex generators are placed on the fin surface (Not punched out) and located at behind the oval tube to help to reduce the pressure loss.The purpose for the use of the delta winglet vortex generators is to generate swirling flow, vortex flow and to enhance the heat transfer coefficient, that leads to the increase in heat transfer rate and thermal performance in comparison with the plain fin or baseline case. The effects of flow attack angles and spacing from V–tip to the center of oval tube in transverse line are investigated numerically for Re = 500 - 2500.

2. Flow description

2.1 Computational model

From Ref. [24], the system of interest is a fin–and–oval–tube compact heat exchanger as depicted in Fig. 1. Fig. 2 shows the schematic diagram of the fin–and–oval–tube heat exchanger with V–Upstream delta winglet vortex generators. The generators are placed behind the oval tube with V–tip pointing upstream. The longitudinal distance between the V–tip to the center of the oval tube in a longitudinal line, equals to 7.78 mm, while transverse distances (a = 3.77, 4.77 and 5.77 mm) and flow attack angles (α = 15^o, 30^o, 45^o and 60^o) are varied. The channel height, H, is set to 3.2 mm, which equals to the winglet height as displayed in Fig. 3. The aspect ratio $\Lambda(4H/c)$ for delta winglet is set to 2. The details of the computational domain are as follows in Table 1.

The computational domain is set at 10H at the entry region to maintain the inlet velocity uniformity and also set at 30H at the exit regimes to ensure a recirculation–free flow.

2.2 Boundary conditions

The assumptions for the fin-and-oval-tube compact heat exchanger with the delta winglet vortex generators are as follows:

- The steady state is used in this computation domain.
- The flow is laminar due to the low inlet velocity flowing though the small fins pitch.
- The fin thickness is taken into account in heat conduction.
- The considered fluid is incompressible with constant properties.

According to the assumptions, the boundary conditions for the current computational model are as follows:

- Uniform velocity and temperature boundary conditions are set for the inlet of the domain, while the exit regime is set as the pressure outlet condition. The symmetry boundaries are used on both sides of the test channel.
- No slip condition and constant wall temperature are applied to the fin–and-oval-tube surfaces.
- The test fluid is air, which maintains constant at 340 K, while the oval tube walls are kept at 300 K.
- The fluid properties are assumed to be constant at the average bulk temperature.
- Due to the range studies are set for Re = 500 - 2500; therefore, the inlet air velocities vary in the range 1.3 to 6.5 m/s.

Table 1. Parameters of the computational domains.

Parameter	Symbol/unit	Value
Computational domain width	B/mm	12.7
Computational domain length	L/mm	64.4
Semi-major diameter of oval tube	R_a/mm	6.28
Semi- minor diameter of oval tube	R_b/mm	3.77
Winglet placed downstream from inlet	Y/mm	17.92
Longitudinal tube pitch	P_l/mm	22
Spanwise tube pitch	P_s/mm	25.4
Fin thickness	F_t/mm	0.33
Fin pitch	F_p/mm	3.2
Number of tube row	n	3
Hydraulic diameter	D_h/mm	3.63
Wall temperature	T_w/K	300
Inlet temperatures of air	T_{in}/K	340
Frontal velocity	u_{in}/m s-1	1.3 - 6.5
Transverse distance from V-tip to the center of the oval tube	a/mm	3.77, 4.77, 5.77
Delta winglet chord length	c/mm	6.4

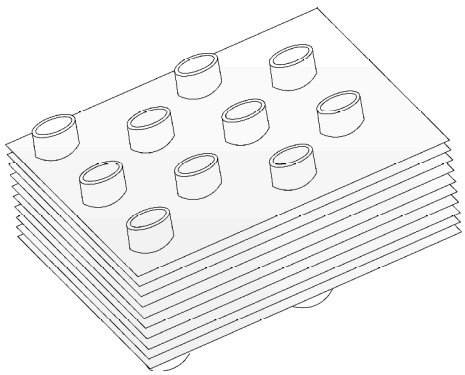

Fig. 1. Fin-and-oval-tube compact heat exchanger.

3. Mathematical foundation and numerical method

From the above assumptions and the boundary conditions, the governing equations for continuity, momentum and energy can be expressed as follows :

Continuity equation:

$$\frac{\partial}{\partial x_i}\left(\rho u_i\right)=0\,. \tag{1}$$

Momentum equation:

$$\frac{\partial}{\partial x_j}\left(\rho u_i u_k\right)=-\frac{\partial P}{\partial x_k}+\frac{\partial}{\partial x_i}\left[\mu\left(\frac{\partial u_k}{\partial x_i}\right)\right]. \tag{2}$$

Energy equation:

$$\frac{\partial}{\partial x_i}\left(\rho u_i T\right)=\frac{\partial}{\partial x_i}\left(\frac{k}{c_p}\frac{\partial T}{\partial x_i}\right). \tag{3}$$

The Reynolds number (*Re*), friction factor (*f*), Nusselt number (*Nu*), and thermal enhancement factor (*TEF*) [30] are presented as follows:

$$\mathrm{Re}=\frac{\rho U_c D_h}{\mu}, \tag{4}$$

$$f=\frac{\left(2\Delta P\right)}{\rho U_c^2}\left(\frac{D_h}{L}\right), \tag{5}$$

$$Nu=\frac{hD_h}{k}, \tag{6}$$

$$TEF=\left(Nu/Nu_0\right)\left(f/f_0\right)^{-1/3}, \tag{7}$$

where U_c, μ, k are the mean velocity in the minimum flow cross section of the flow channel, viscosity and the thermal conductivity, respectively. D_h is the hydraulic diameter, Δp the pressure drop across computation domain, L the fin length along the flow direction and H the height of the channel flow. The Nu and Nu_0 area-average Nusselt number and average Nusselt number of plain fin, respectively.

The convective terms in the governing equations for momentum and energy are discretized with Powerlaw scheme and QUICK scheme, respectively. The SIMPLE algorithm has been applied on the coupling among pressure and velocity. The convergence criteria for the velocities and temperature are arranged by the residual less than $10^{-5}$and 10^{-9}, respectively.

4. Results and discussion

4.1 Validation of the computational domain

Although the numerical method can help to save time and cost for investigation when compared with the experimental investigation, the accuracies of the computational domain are very important. The verifications of the current computational domain are considered in two parts: grid independence and comparison with the experimental results on both Nusselt number and friction factor.

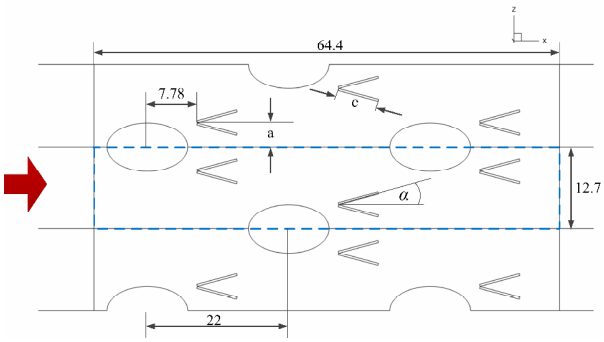

Fig. 2. Schematic diagram of computational domain.

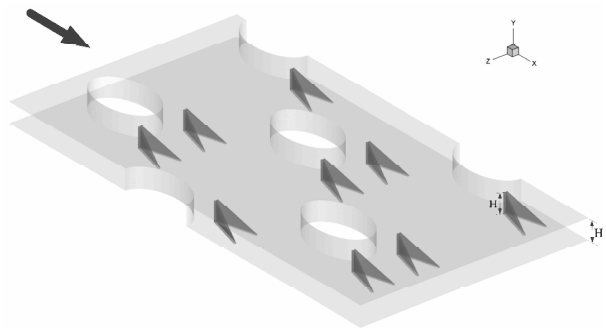

Fig. 3. Fin-and-oval-tube heat exchanger with delta winglet vortex generators.

The grid systems test is done by comparing the results from various numbers of grid cells. The three sets of grid, 150000, 310000 and 450000 cells, are applied to the current computational model. The numerical results show that the relative errors of the Nusselt number and friction factor are less than 1.1% and 1.2%, respectively, when increasing the number of grid cells from 150000 to 310000. Hence, there is no advantage for increasing grid cells. The current computational domain uses about 150000 cells of the grid.

Comparisons between the numerical and the experimental results under similar conditions for baseline case are presented as Figs. 4(a) and (b) for Nusselt number and friction factor, respectively. The results are found to be in excellent agreement with experimental values obtained from the open literature [24] for both the Nusselt number and the friction factor, less than 10% deviations. This means that the computational domain is reliable to predict heat transfer behaviors, flow configurations and thermal performance in the fin–and–oval–tube compact heat exchangers.

4.2 Flow configuration

It is necessary to understand the flow configurations in the fin–and–tube heat exchanger with the V–Upstream delta winglet vortex generators. The flow configurations in the

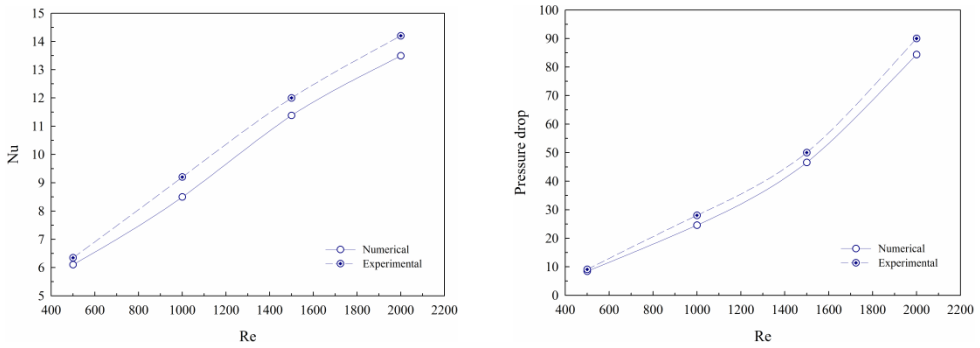

(a) (b)

Fig. 4. Experimental-numerical comparison for model validations: (a) Nusselt number; (b) pressure drop.

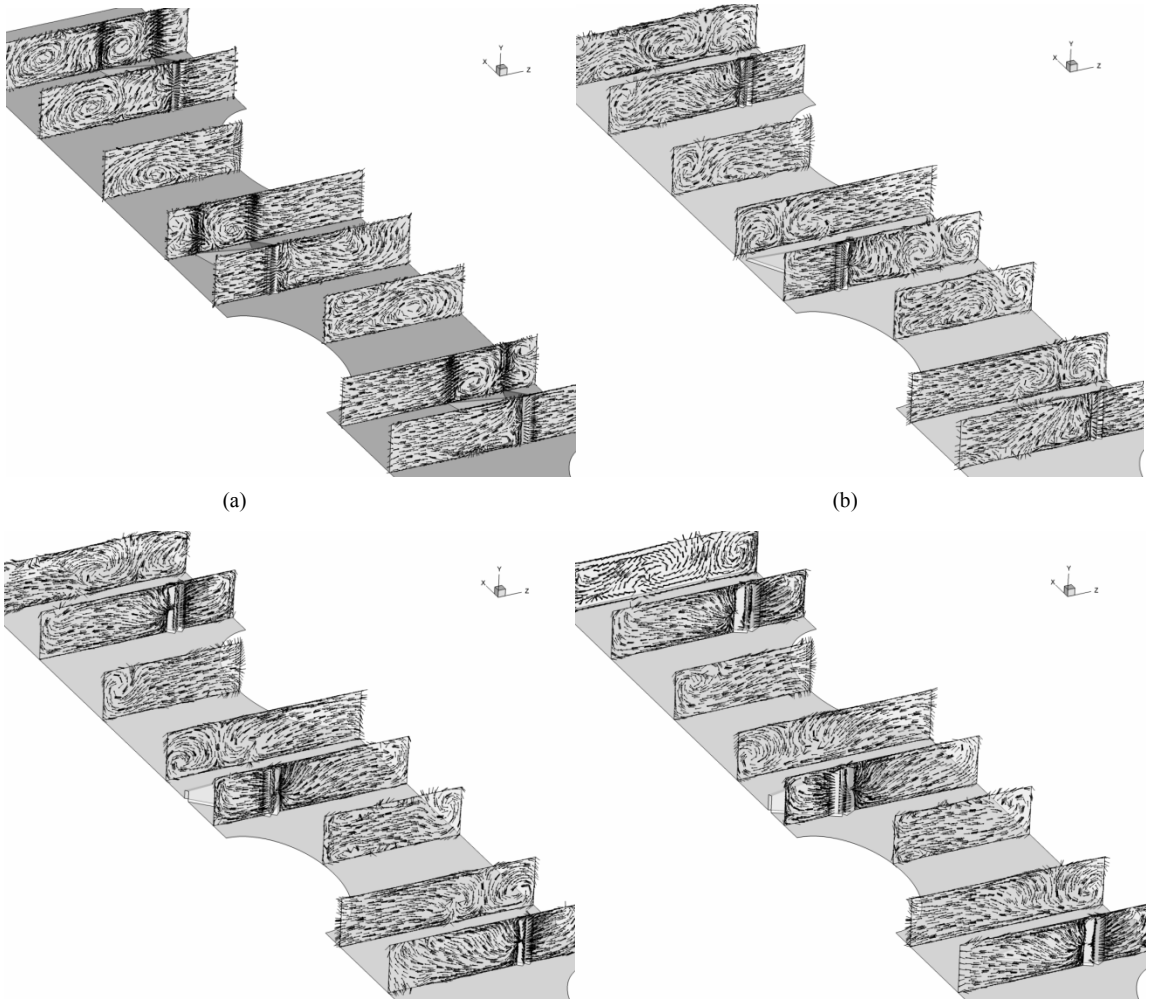

(a) (b)

(c) (d)

Fig. 5. Velocity vectors in transverse planes for (a) 15°; (b) 30°; (c) 45°; (d) 60° at Re = 1000 and a = 3.77 mm.

compact heat exchanger are presented in terms of velocity vectors in transverse planes at various positions and the longitudinal vortex flows over the fin–and–tube heat exchanger. In general, the use of the delta winglet vortex generators can help to induce the vortex flows and swirling flows when compared with the smooth fin. The presence of the vortex flows leads to a better mixing of temperature between near the oval–tube walls and at the center of the test channel result in a higher heat transfer rate and thermal performance.

Figs. 5(a)-(d) illustrate the velocity vector in transverse planes of the fin–and–oval–tube heat exchanger with the delta winglet vortex generators for α = 15°, 30°, 45° and 60°, respec-

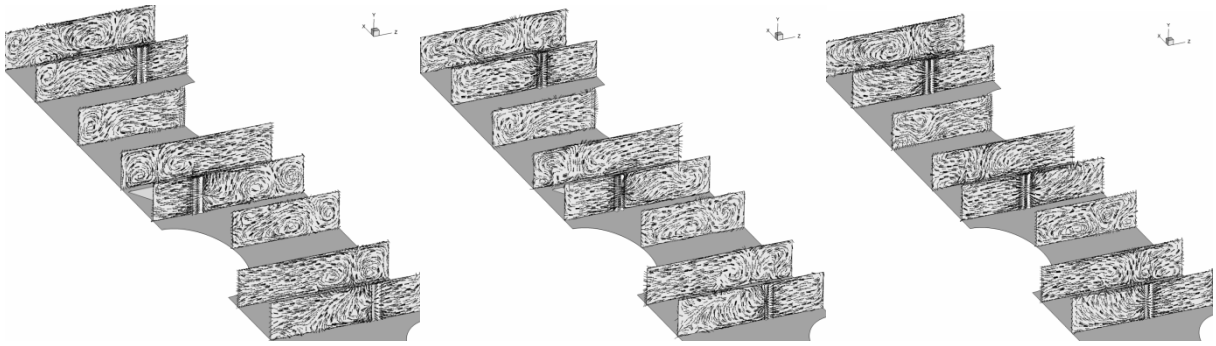

(a) (b) (c)

Fig. 6. Velocity vectors in transverse planes for (a) a = 3.77 mm; (b) a = 4.77 mm; (c) a = 5.77 mm at Re = 1500 and $\alpha = 30^{o}$.

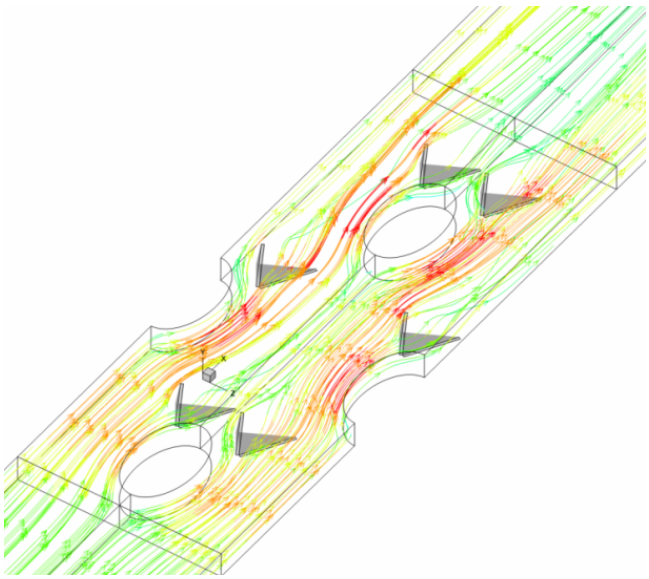

Fig. 7. Streamlines over fin-and-oval-tube heat exchanger for a = 3.77 mm at Re = 1000 and $\alpha = 30^{o}$.

tively, at Re = 1000 and a = 3.77 mm. It is clearly seen that vortex flows appear when the flow passes the delta winglet vortex generators for all cases, especially at the trailing end of the vortex generators. The positions of the vortex core are found to be changed depending on flow attack angle of the delta winglet vortex generators.

The effects of the distance between V–tip to the center of the oval–tube in transverse line, a, on the flow structure are displayed in Figs. 6(a)-(c) for a = 3.77, 4.77, and 5.77 mm, at $\alpha = 30^{o}$ and Re = 1500, respectively. As seen, the flow configurations at different a values performed similarly; the vortex flows are performed when passing the delta winglet vortex generators, but slight differences in the vortex core positions.

The longitudinal vortex flows over the fin–and–oval–tube heat exchanger with the delta winglet vortex generators are shown in Fig. 7 for a = 3.77 mm, Re = 1000 and $\alpha = 30^{o}$. The fluid flows become swirling when passing the V–tip of the first pair winglet vortex generators due to the pressure differences, after that the fluid flows faster and impinges at the second row of the oval–tubes. This phenomenon appears again between the second pair winglet vortex generators and the third row of the oval–tube. In addition, the swirling flows, vortex flows and impinging flow over the oval–tubes are main factors for enhancing heat transfer in the heat exchanger.

4.3 Velocity distribution

The variations of velocity in the compact heat exchanger with the delta winglet vortex generators are presented in term of the x–velocity distributions at the middle of the x–z plane. The numerical results are divided into the effect of the flow attack angle and the effect of the distance between V–tip and the center of the oval–tube in transverse line.

Figs. 8(a)-(d) show the velocity distributions at the middle of the x–z plane for $\alpha = 15^{o}$, 30^{o}, 45^{o} and 60^{o}, respectively, for Re = 1000 and a = 3.77 mm. In general, the velocity distributions at the entrance region show uniformity. After the flow passes the first pair of the delta winglet vortex generators, the velocity of the flow increases at near the second row of the oval tubes regimes, but the velocity behind the delta winglet

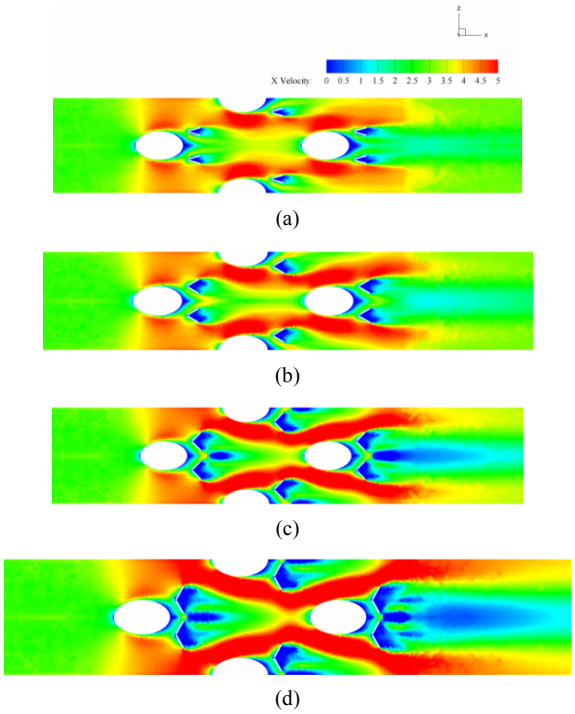

Fig. 8. X-velocity distributions for (a) 15°; (b) 30°; (c) 45°; (d) 60°at *Re* = 1000 and *a* = 3.77 mm.

vortex generators is seen to decrease. These behaviors are found again between the second row of the delta winglet vortex generators and the third row of the oval tubes. The variations of the flow attack angles show a similar profile of the velocity distributions.

The effect of the flow attack angles, $\alpha = 60^{o}$, provides the highest velocity values, while $\alpha = 15^{o}$ performs the lowest values at similar conditions, *Re* = 1000 and *a* = 3.77 mm. The reason for this may be that $\alpha = 60^{o}$ produces the highest vortex intensity or turbulence level in comparison to other cases. In addition, the rise of the flow attack angle results in the increase in the vortex intensity and also provides the highest values of the velocity distributions over the fin–and–oval–tube compact heat exchanger.

Figs. 9(a)-(c) present the velocity distributions in the middle of the x–z plane for *a* = 3.77, 4.77 and 5.77 mm, respectively, at *Re* = 1500 and $\alpha = 30^{o}$. Generally, high values of the velocity are found at near the two side curve of the second and third rows of the oval tubes. The difference in the distance between V–tip of the delta winglet vortex generators and the center of the oval–tube leads to slight difference of the velocity pattern.

4.4 Heat transfer behavior

The heat transfer characteristics are presented in forms of the temperature distributions at the middle of the x–z plane, the temperature distributions in transverse planes and the local Nusselt number distributions over the oval–tube walls. The influences of the flow attack angles and *a* value are shown in this section.

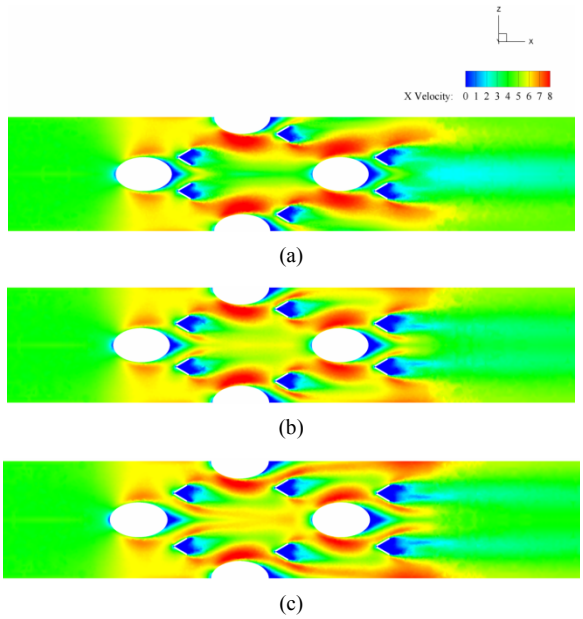

Fig. 9. X-velocity distributions for (a) *a* = 3.77 mm; (b) *a* = 4.77 mm; (c) *a* = 5.77 mm at *Re* = 1500 and $\alpha = 30^{o}$.

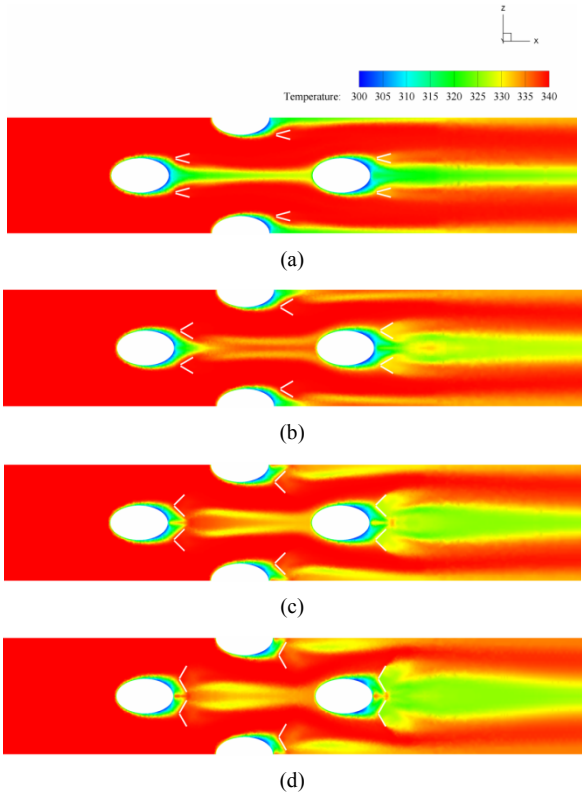

Fig. 10. Temperature distributions in x-z plane for (a) 15°; (b) 30°; (c) 45°; (d) 60° at *Re* = 1000 and *a* = 3.77 mm.

Figs. 10(a)-(d) illustrate the temperature distributions at the middle of the x–z plane for $\alpha = 15^{o}$, 30^{o}, 45^{o} and 60^{o}, respectively, at *Re* = 1000 and *a* = 3.77 mm. As seen, $\alpha = 60^{o}$ per-

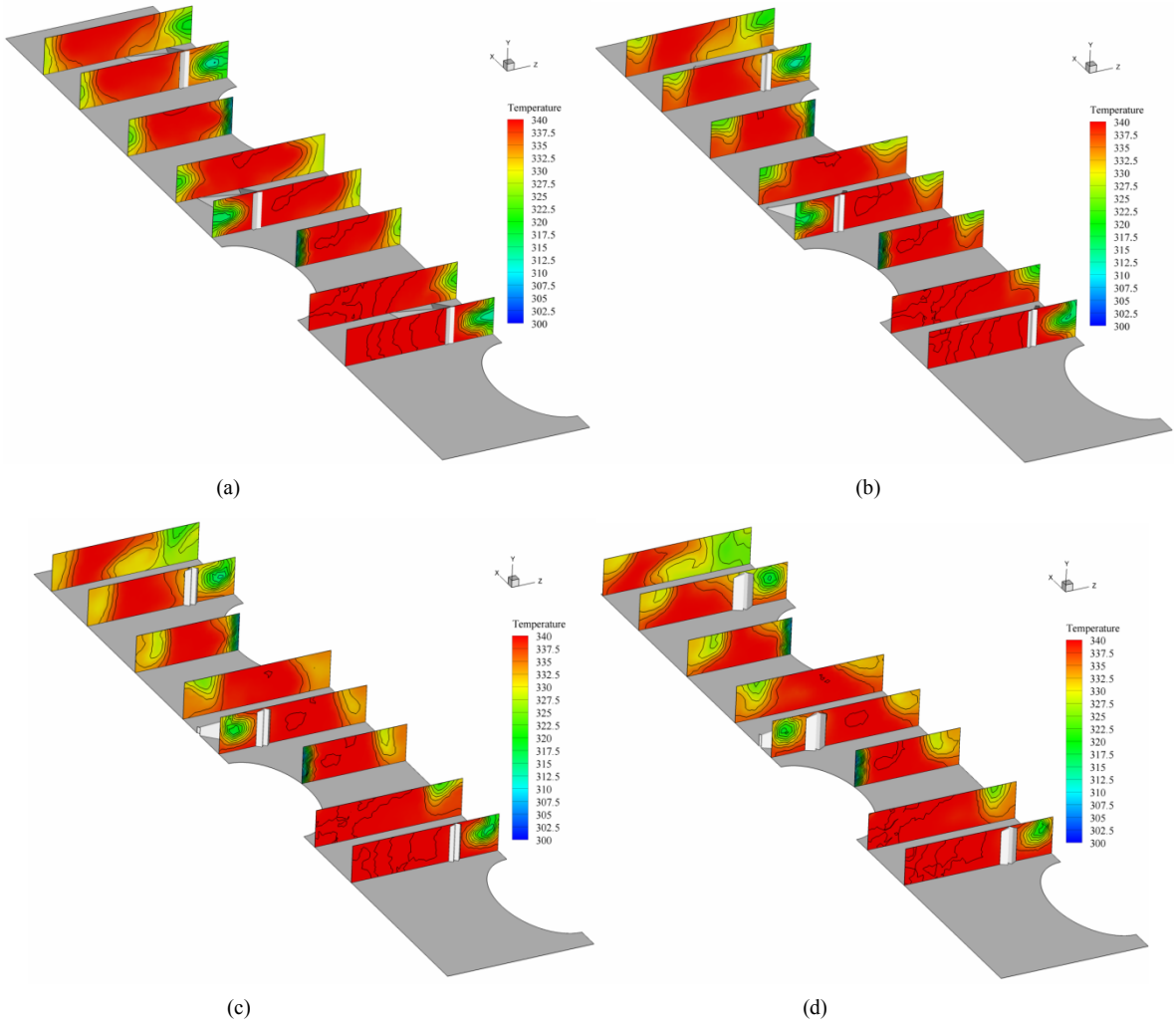

Fig. 11. Temperature distributions in transverse planes for (a) 15°; (b) 30°; (c) 45°; (d) 60° at Re = 1000 and a = 3.77 mm.

forms the best temperature distribution, while the case of α = 15° provides the opposite result. This may be that α = 60° produces the highest vortex intensity that leads to the best mixing of the fluid flow over the test channel. The case of α = 45° gives better temperature distributions than α = 30°.

The temperature distributions in transverse planes at various positions are presented in Figs. 11(a)-(d) for α = 15°, 30°, 45° and 60°, respectively, at Re = 1000 and a = 3.77 mm. Good mixing of the fluid flow is found at seventh and eighth plane downstream from the inlet of the test channel in all cases. The better mixing is by the vortex flow or the swirling flow that is created from the delta winglet vortex generators. The numerical results agree well with the temperature distributions at the middle of the x–z plane in the previous part; the case of α = 60° gives the best mixing of the fluid flow in comparison with other cases, while α = 15° provides the reverse result. Figs. 12(a)-(c) present the temperature distributions at the middle of the x–z plane at Re = 1500 and α = 30° for a = 3.77, 4.77 and 5.77 mm, respectively. At similar conditions, a = 3.77 mm shows the greatest mixing of the fluid flow, especially, at behind the third row of the oval–tube, while a = 4.77 mm performs better mixing than a = 5.77 mm.

The temperature distributions in transverse plane are presented in Figs. 13(a)-(c) for a = 3.77, 4.77 and 5.77 mm at Re = 1500 and α = 30°. Considering at the last plane of each case, the case of a = 3.77 mm gives the best fluid mixing, while a = 4.77 and 5.77 mm show very close pattern of the temperature distributions.

The local Nusselt number distributions over the oval tube walls are displayed in the Figs. 14(a)-(d) for α = 15°, 30°, 45° and 60°, respectively, at Re = 1000 and a = 3.77 mm. In general, the delta winglet vortex generators give higher heat transfer rate than the baseline case, especially, at the leading curve of the second row for the oval–tubes. As seen from the figures, α = 60° provides the highest Nusselt number, while α = 15° gives the lowest values. Due to the high level of vortex strength generated from α = 60° and also the best fluid mixing, therefore, α = 60° case gives the highest heat transfer rate.

Figs. 15(a)-(c) present the local Nusselt number distributions over the oval tube walls for α = 30° and Re = 1500 of a =

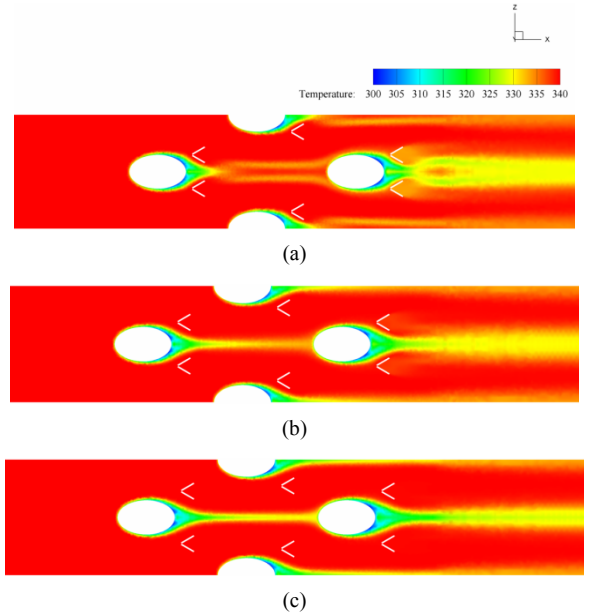

Fig. 12. Temperature distributions in x-z plane for (a) a = 3.77 mm; (b) a = 4.77 mm; (c) a = 5.77 mm at Re = 1500 and α = 30°.

3.77, 4.77 and 5.77 mm, respectively. The peak of heat transfer augmentation is found at the leading curve in the second row of the oval tubes.

4.5 Performance assessment

As the previous numerical results, it is found that the delta winglet vortex generators can help to enhance heat transfer rate due to the vortex flow induced from the vortex generators. The uses of the generators not only increase in heat transfer rate, but also increase in the pressure loss in the compact heat exchanger. Therefore, the thermal performance in the heat system should be considered on both the heat transfer augmentation and the increase in the friction factor.

The performance evaluations are divided into three parts: heat transfer, pressure loss and thermal performance. The heat transfer augmentation is shown in terms of the average Nusselt number, Nu, and the average Nusselt number ratio, Nu/Nu_0, while the pressure loss is presented in forms of the average friction factor, f, and the average friction factor ratio, f/f_0. The thermal performance is shown as the thermal enhancement factor, TEF, with the Reynolds number.

Figs. 16(a)-(c) illustrate the variations of the Nusselt number with the Reynolds number at various flow attack angles for a = 3.77, 4.77 and 5.77 mm, respectively.The increase of the Nusselt number is due to the augmentation on the heat transfer coefficient when increasing the Reynolds number value. In range studies, the increase in the Nusselt number is found with increasing Reynolds number for all cases. The case of α = 60° performs the highest of the Nusselt number, while the lowest values are seen for α = 15°. The case of α = 45° gives a higher heat transfer rate than α = 30° for all Reynolds

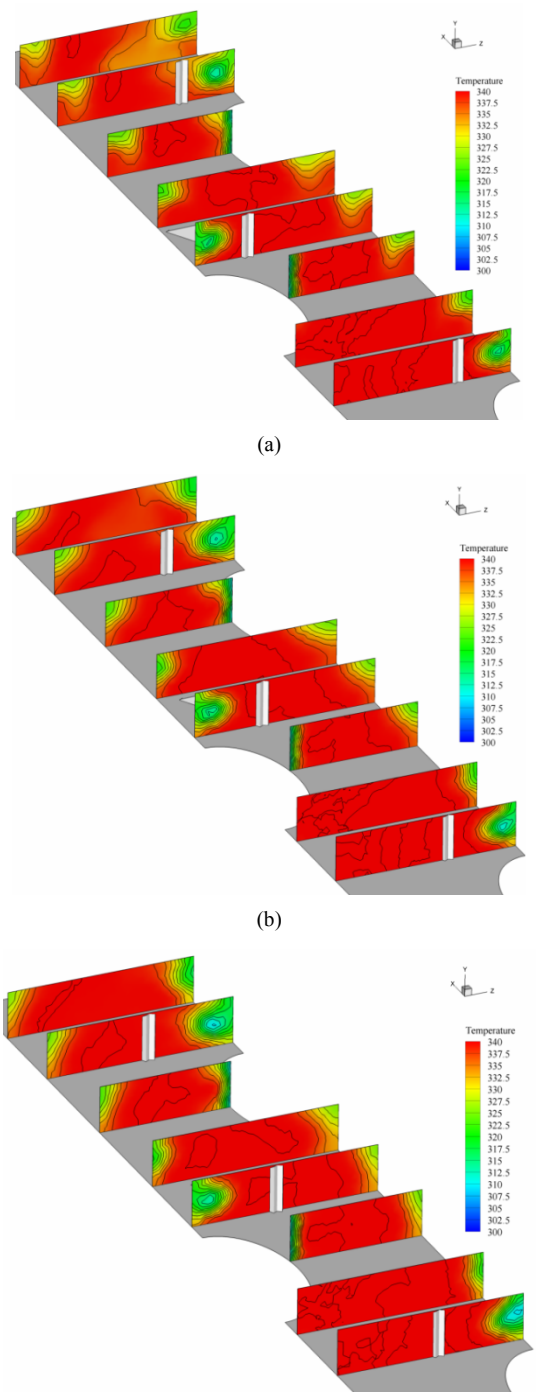

Fig. 13. Temperature distributions in transverse planes for (a) a = 3.77 mm; (b) a = 4.77 mm; (c) a = 5.77 mm at Re = 1500 and α = 30°.

number values. The reason of this may be that the high flow attack angle can generate a turbulence level, vortex strength and impinging flows higher than the low attack angle.

For a = 3.77 mm, the case of α = 60° gives higher heat transfer rate than α = 45°, 30° and 15° around 4.71%, 8.38% and 16.23%, respectively, at Re = 2500. The maximum Nus-

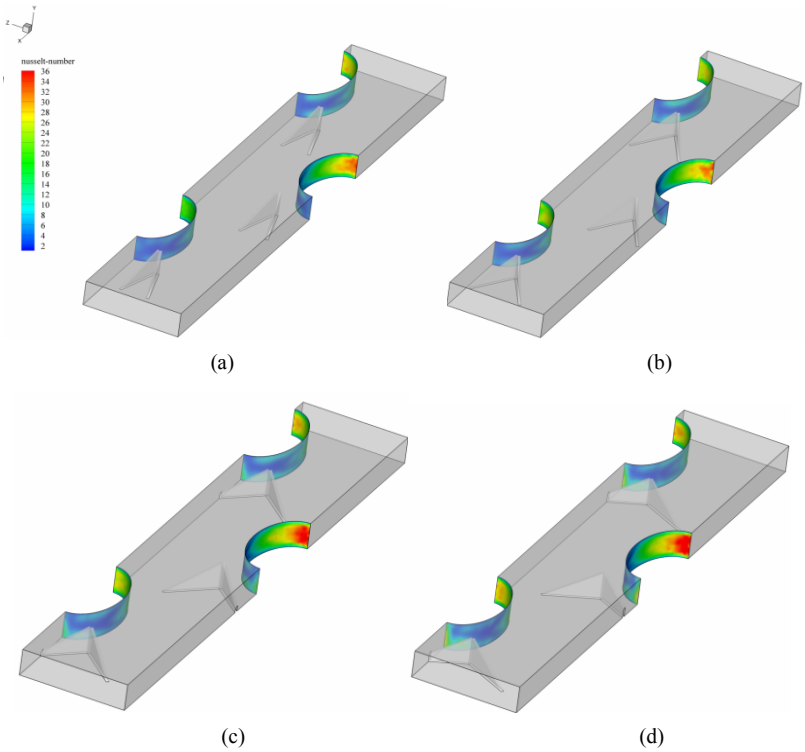

Fig. 14. Local Nusselt number distributions at oval tubes for (a) 15°; (b) 30°; (c) 45°; (d) 60° at Re = 1000 and a = 3.77 mm.

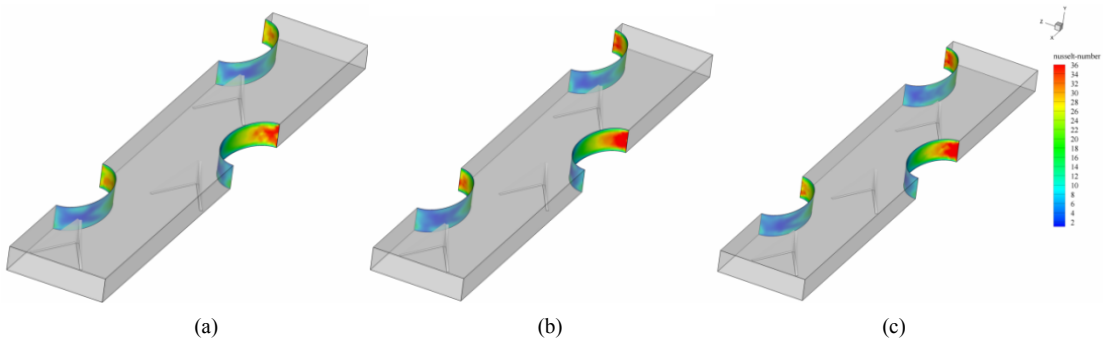

Fig. 15. Local Nusselt number distributions at oval tubes for (a) a = 3.77 mm; (b) a = 4.77 mm; (c) a = 5.77 mm at Re = 1500 and α = 30°.

selt number values are found at the highest Reynolds number about 19.1, 18.2, 17.5 and 16, respectively, for α = 60°, 45°, 30° and 15°.

For a = 4.77 mm, Nusselt number produces nearly values as case of a = 3.77 mm for all the flow attack angles. The peak of the Nusselt number is found to be around around 19.1, 18, 17 and 16.5, respectively, for α = 60°, 45°, 30° and 15° at Re = 2500. The α = 60° case gives a higher Nusselt number than the α = 45°, 30° and 15° around 5.76%, 11% and 13.61%, respectively.

For a = 5.77 mm, the case of α = 60° provides nearly value as a = 3.77 and 4.77 mm, which the peak of the Nusselt number is around 19 at the highest Reynolds number. The α = 45° case provides slightly higher than the α = 30° and 15° around 1.16% and 2.34%, respectively, considering at the highest Reynolds number. The maximum Nusselt numbers of the α = 45°, 30° and 15° cases are found to be about 17.2, 17 and 16.8, respectively.

The variations of the Nu/Nu_0 with the Reynolds number for a = 3.77, 4.77 and 5.77 mm are shown in Figs. 17(a)-(c), respectively, at various flow attack angles. The delta winglet vortex generators give a higher heat transfer rate than the smooth fin with no generators for all cases. The rise of the flow attack angle leads to the increase in the Nu/Nu_0 for all a values. The vortex flows, impinging flow and small vortices, created by the delta winglet vortex generators, are the cause for the heat transfer augmentation over the smooth case, especially, at a high flow attack angle.

For a = 3.77 mm, the Nu/Nu_0 tends to increase when $Re \leq$ 2000, but decreases when Re > 2000. The peak of the Nu/Nu_0 is found at the Re = 2000 around 1.55, 1.48, 1.38 and 1.28 for α = 60°, 45°, 30° and 15°, respectively. For a = 4.77 mm, simi-

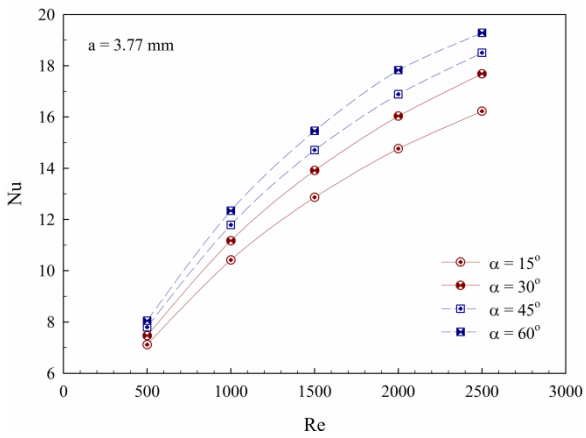

(a)

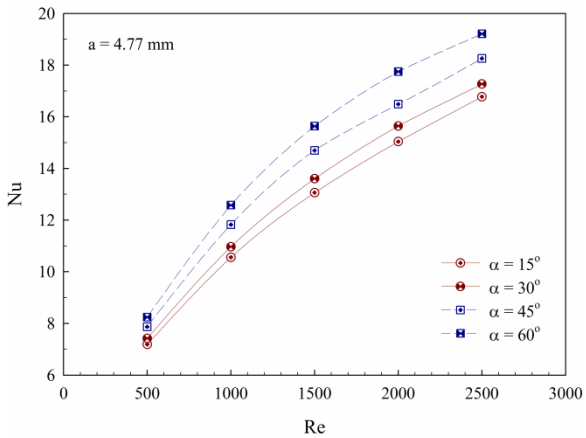

(b)

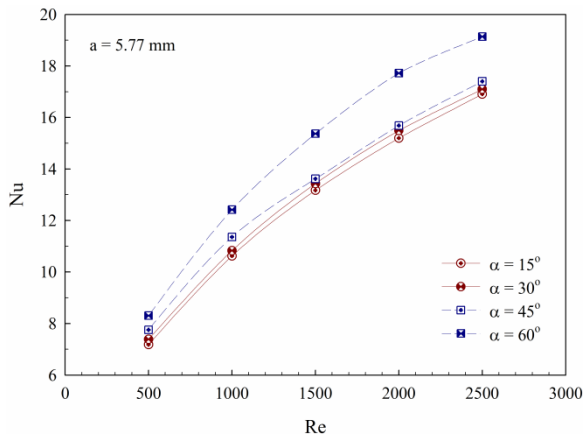

(c)

Fig. 16. The variations of Nusselt number with Reynolds number for (a) a = 3.77 mm; (b) a = 4.77 mm; (c) a = 5.77 mm.

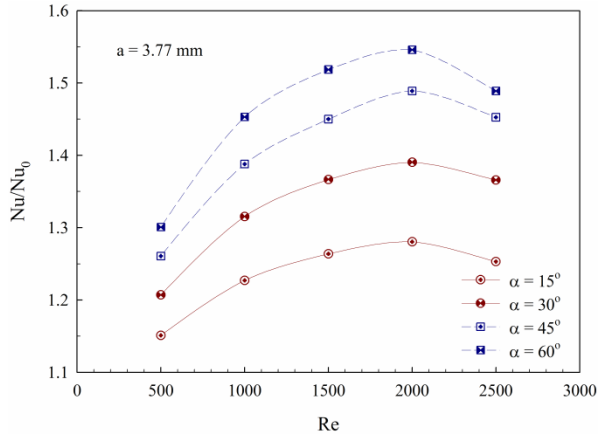

(a)

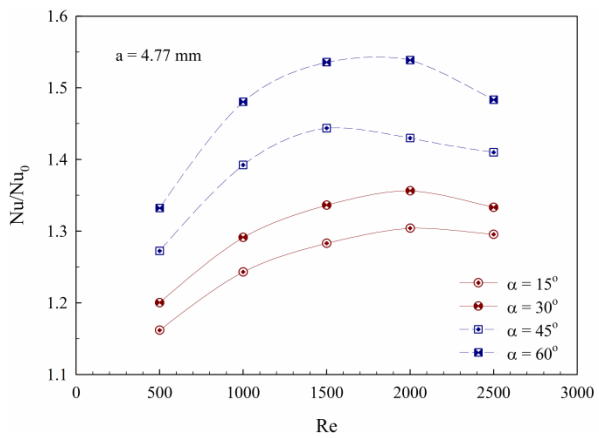

(b)

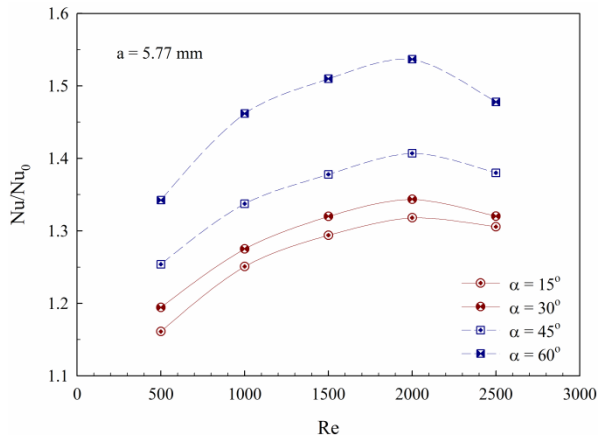

(c)

Fig. 17. The variations of Nu/Nu_0 with Reynolds number for (a) a = 3.77 mm; (b) a = 4.77 mm; (c) a = 5.77 mm.

lar trends as a = 3.77 mm are found in this case, except for α = 45°, the decrease trend of the Nu/Nu_0 appears when the Reynolds number is higher than 1500. The maximum values of the Nu/Nu_0 are around 1.54, 1.44, 1.35 and 1.29 for α = 60°, 45°, 30° and 15° at Re = 2000, 1500, 2000 and 2000, respectively. The case of a = 5.77 mm gives a similar trend of the Nu/Nu_0 as a = 3.77 mm. The optimum values of the Nu/Nu_0 are around 1.53, 1.4, 1.33 and 1.3 for α = 60°, 45°, 30° and 15°, respectively, at Re = 2000.

The variations of the friction factor with the Reynolds number at various the flow attack angles are displayed in Figs. 18(a)-(c) for a = 3.77, 4.77 and 5.77 mm, respectively. As

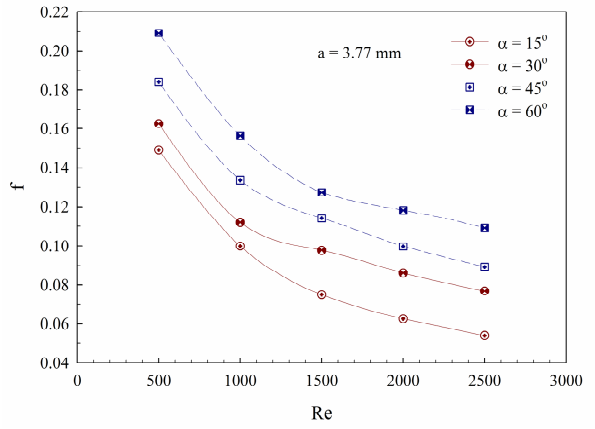

(a)

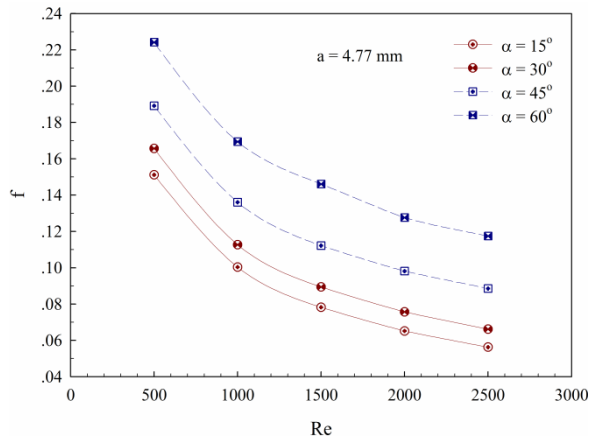

(b)

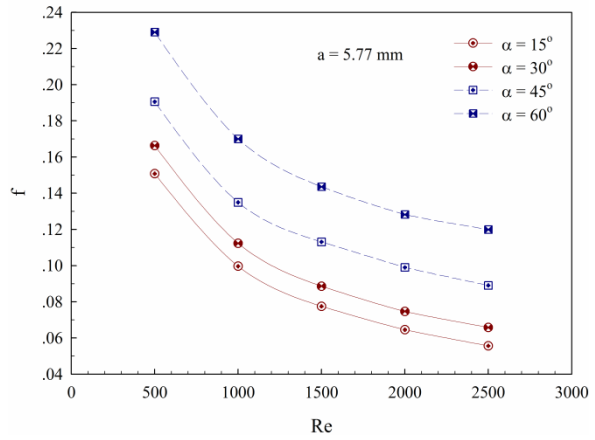

(c)

Fig. 18. The variations of friction factor with Reynolds number for (a) a = 3.77 mm; (b) a = 4.77 mm; (c) a = 5.77 mm.

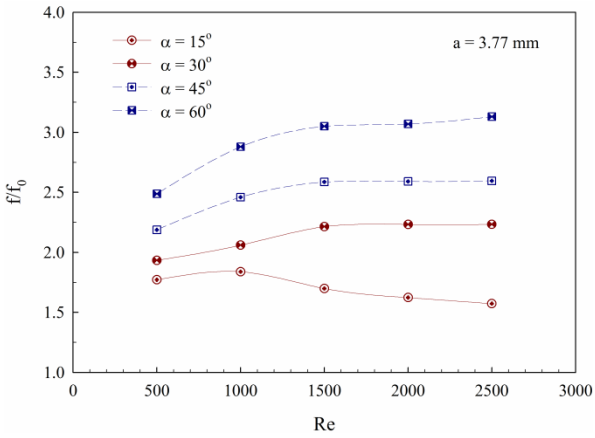

(a)

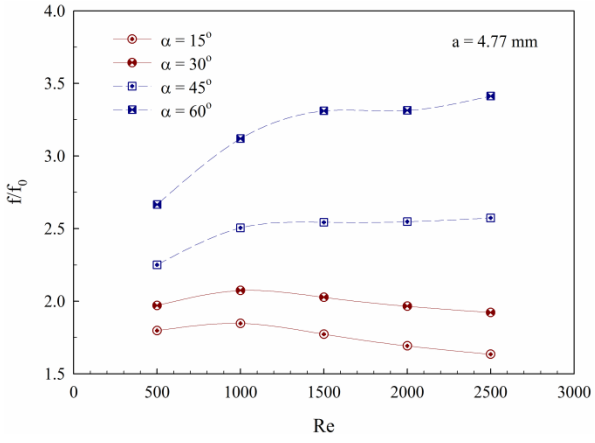

(b)

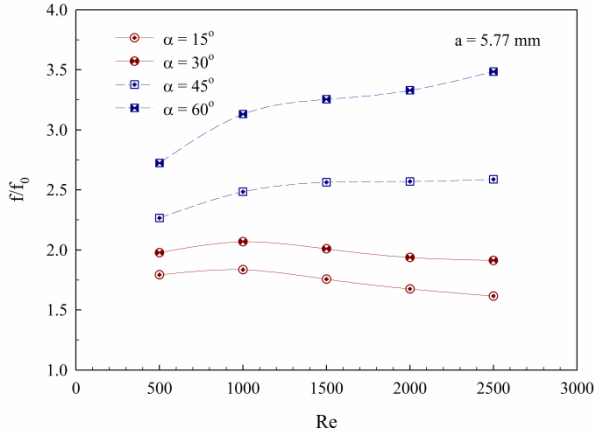

(c)

Fig. 19. The variations of f/f_0 with Reynolds number for (a) a = 3.77 mm; (b) a = 4.77 mm; (c) a = 5.77 mm.

seen, the friction factor tends to decrease with the rise of Reynolds number for all cases. The case of α = 60° gives the highest friction factor, while α = 15° gives the lowest values of the friction factor for all Reynolds numbers. In addition, the rise of the flow attack angle results in an extreme increase in the friction factor. The case of a = 3.77 mm gives the maximum friction factor around 0.21, 0.18, 0.16 and 0.15 for α = 60°, 45°, 30° and 15°, respectively, at the lowest Reynolds number, Re = 500. The case of a = 4.77 mm provides a higher friction factor than a = 3.77 mm around 6.67%, 3.16% and 2.38%, respectively, for α = 60°, 45° and 30°. The friction factor of α = 15° shows nearly values at a = 3.77 and 4.77 mm

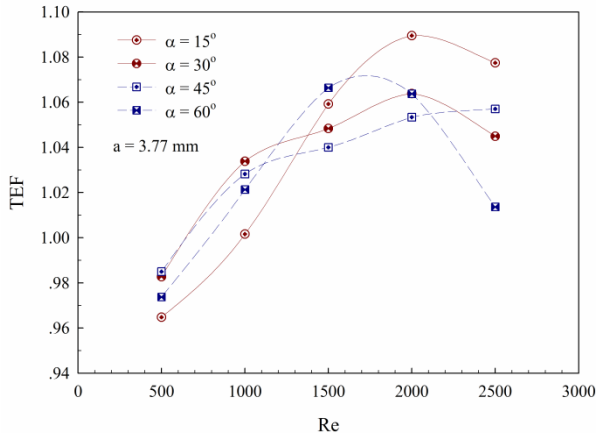

(a)

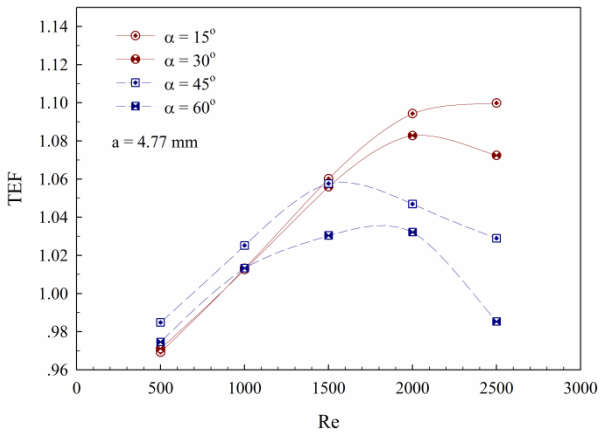

(b)

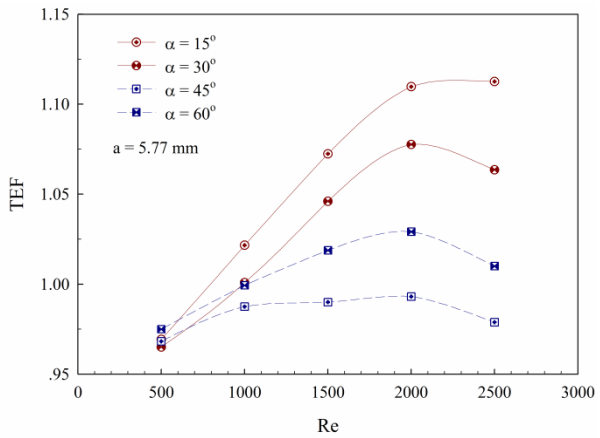

(c)

Fig. 20. The variations of *TEF* with Reynolds number for (a) a = 3.77 mm; (b) a = 4.77 mm; (c) a = 5.77 mm.

for all Reynolds numbers. The peak values of the friction factor are around 0.23, 0.19, 0.17 and 0.15 for $\alpha = 60^o$, 45^o, 30^o and 15^o, respectively, at Re = 500 and a = 5.77 mm.

Comparisons of the friction factor with the smooth fin are presented in Figs. 19(a)-(c) for a = 3.77, 4.77 and 5.77 mm, respectively. The delta winglet vortex generators produce higher friction factor than the baseline case, especially at the large flow attack angles $\alpha = 60^o$ and 45^o. The augmentations in the friction factor are around 1.5 - 3.1, 1.6 - 3.4 and 1.7 - 3.4 times over than the baseline case for a = 3.77, 4.77 and 5.77 mm, respectively.

The thermal performance, considered from the increase on both the heat transfer and friction factor in the test section, is presented in Figs. 20(a)-(c), respectively, for a = 3.77, 4.77 and 5.77 mm in terms of the thermal enhancement factor, *TEF*, with the Reynolds number. The use of *TEF* is referred from Ref. [30] by considering the test section as the channel heat exchanger. In range studies, the *TEF* is found around 0.965 - 1.090, 0.970 - 1.100 and 0.960 - 1.120 for a = 3.77, 4.77 and 5.77 mm, respectively. The optimum *TEF* is to be about 1.12 at Re = 2500, $\alpha = 15^o$ and a = 5.77 mm.

5. Conclusions

Three-dimensional numerical investigations for the flow configurations, heat transfer characteristics and thermal performance in the fin–and–oval–tube compact heat exchanger with the delta winglet vortex generators are presented. The delta winglet vortex generator pairs like V–ribs are placed on the fin surface at behind the three rows of the oval–tubes with pointing upstream called "V–Upstream." The effects of the flow attack angles, α = 15^o, 30^o, 45^o and 60^o, the distances between V–tip to the center of the oval–tube in transverse, a = 3.77, 4.77 and 5.77 mm are investigated for Reynolds number based on the hydraulic diameter of the test channel, Re = 500 - 2500. The main finding can be concluded as follows:

The use of the V–Upstream delta winglet vortex generators can create the vortex flows and swirling flow that leads to better mixing of the fluid flow over the test channel and also improve the heat transfer rate. The peaks of heat transfer regimes are found at the leading curve of the oval-tube, especially, at the second row tube. The delta winglet vortex generators not only increase the heat transfer rate, but also increase the pressure loss in the heat transfer system.

The rise of the flow attack angle results in the augmenting of heat transfer rate and friction factor. The case of $\alpha = 60^o$ performs the highest on both the Nusselt number and the friction factor while the case of $\alpha = 15^o$ gives the lowest values.

Differences in the distance between the V–tip to the center of the oval–tube lead to slight differences in the Nusselt number and the friction factor values.

In range studies, the augmentation of the heat transfer rate is found to be around 1.15 - 1.55 times over the smooth plain fin, while the enhancement of the friction factor is around 1.5 - 3.4 times higher than the base case with no delta winglet vortex generators.

The thermal enhancement factor is found to be optimum at Re = 2500, a = 5.77 mm and $\alpha = 15^o$ around 1.12. The use of the delta winglet vortex generators yields a *TEF* around 0.96 - 1.12 depending on the Reynolds number, the flow attack angle and the distance between V–tip to the center of the oval–tube.

Acknowledgment

The authors would like to thank King Mongkut's Institute of Technology Ladkrabang research fund and Assoc. Prof. Dr. Pongjet Promvonge for research suggestions.

Nomenclature

a : Distance between V-tip to the center of the oval tube in transverse line (mm)
B : Channel width (m)
c : Delta winglet chord length (m)
D_h : Hydraulic diameter
f : Friction factor
F_p : Fin pitch (m)
F_t : Fin thickness (m)
h : Heat transfer coefficient (W/m^2 K)
H : Channel height (m)
k : Thermal conductivity (W/m K)
L : Flow length (m)
n : Tube row number
Nu : Nusselt number, $(hD_h)/k$
P : Pressure (Pa)
P_l : Longitudinal tube pitch (m)
P_s : Spanwise tube pitch (m)
Δp : Air-side pressure drop (Pa)
R_a : Semi-major diameter
R_b : Semi-minor diameter
Re : Reynolds number, $Re = \rho U_c D_h/\mu$
T : Temperature (K)
TEF : Thermal enhancement factor, $TEF = (Nu/Nu_0)(f/f_0)^{-(1/3)}$
u, v, w : Velocity components (m/s)
u_{in} : Frontal velocity (m/s)
U_c : Velocity at the minimum cross sectional area, A_c (m/s)
x, y, z : Cartesian coordinates

Greek symbols

α : Angle of attack
μ : Dynamic viscosity (Pa s)
υ : Kinematic viscosity (m^2/s)
ρ : Density (kg/m^3)
k : Thermal conductivity (W/m K)
Λ : Winglet aspect ratio

Subscripts

in : Inlet parameter
w : Wall
0 : Smooth fin

References

[1] W. R. Pauley and J. K. Eaton, The effect of embedded longitudinal vortex array on turbulent boundary layer heat transfer, *J. Heat Transfer*, 116 (1994) 871-85.
[2] D. E. Wroblewski and P. A. Eibeck, Measurements of turbulent heat transfer in a boundary layer with an embedded streamwise vortex, *Int. J. Heat Mass Transfer*, 34 (7) (1991) 1617-1631.
[3] E. Kim and J. S. Yang, An experimental study of heat transfer characteristics of a pair of longitudinal vortices using color capturing technique, *Int. J. Heat Mass Transfer*, 45 (2002) 3349-3356.
[4] N. Depaiwa, T. Chompookham and P. Promvonge, Thermal enhancement in a solar air heater channel using rectangular winglet vortex generators, *International conference on energy and sustainable development* (2010) 1-7.
[5] W. Qiuwang, C. Qiuyang, W. Ling, Z. Min, H. Yanping and X. Zejun, Experimental study of heat transfer enhancement in narrow rectangular channel with longitudinal vortex generators, *Nuclear Eng. Design*, 237 (2007) 686-693.
[6] M. Jian, P. H. Yan, H. Jun, L. W. Yan and W. W. Qiu, Experimental investigations on single-phase heat transfer enhancement with longitudinal vortices in narrow rectangular channel, *Nuclear Eng. Design*, 240 (2010) 92-102.
[7] C. Min, C. Qi, X. Kong and J. Dong, Experimental study of rectangular channel with modified rectangular longitudinal vortex generators, *Int. J. Heat Mass Transfer*, 53 (2010) 3023-3029.
[8] C. Habchi, S. Russeil , D. Bougeard, J. L. Harion, T. Lemenand, D. D. Valle and H. Peerhossaini, Enhancing heat transfer in vortex generator-type multifunctional heat exchangers, *Appl. Therm. Eng.*, 38 (2012) 14-25.
[9] B. A. Sarac and T. Bali, An experimental study on heat transfer and pressure drop characteristics of decaying swirl flow through a circular pipe with a vortex generator, *Exp. Therm. Fluid Sci*., 32 (2007) 158-165.
[10] J. M. Wu and W. Q. Tao, Numerical study on laminar convection heat transfer in a rectangular channel with longitudinal vortex generator Part A: Verification of field synergy principle, *Int. J. Heat Mass Transfer*, 51 (2008) 1179-1191.
[11] J. M. Wu and W. Q. Tao, Numerical study on laminar convection heat transfer in a channel with longitudinal vortex generator. Part B: Parametric study of major influence factors, *Int. J. Heat Mass Transfer*, 51 (2008) 3683-3692.
[12] G. Biswas and H. Chattopadhyay, Heat transfer in channel with built-in wing-type vortex generators, *Int. J. Heat Mass Transfer*, 35 (4) (1992) 803-814.
[13] S. T. Ahmed, W. S. Mohammed and J. H. Laith, Numerical investigation into velocity and temperature fields over smooth and rough ducts for several types of turbulators, *J. Eng. Technology*, 25 (10) (2007) 1110-1128.
[14] S. R. Hiravennavar, E. G. Tulapurkara and G. Biswas, A note on the flow and heat transfer enhancement in a channel with built-in winglet pair, *Int. J. Heat Fluid Flow*, 28 (2007) 299-305.
[15] G. Biswas, P. Deb and S. Biswas, Generation of longitudinal streamwise vortices-a device for improving heat exchanger design, *J. Heat Transfer*, 116 (1994) 588-597.

[16] A. Sohankar, Heat transfer augmentation in a rectangular channel with a vee-shaped vortex generator, *Int. J. Heat Fluid Flow*, 28 (2007) 306-317.
[17] J. S. Leu, Y. H. Wu and J. Y. Jang, Heat transfer and fluid flow analysis in plate-fin and tube heat exchangers with a pair of block shape vortex generators, *Int. J. Heat Mass Transfer*, 47 (2004) 4327-4338.
[18] A. D. Sommers and A. M. Jacobi, Air-side heat transfer enhancement of a refrigerator evaporator using vortex generation, *Int. J. Refrig*., 28 (2005) 1006-1017.
[19] S. M. Pesteei, P. M. V. Subbarao and R. S. Agarwal, Experimental study of the effect of winglet location on heat transfer enhancement and pressure drop in fin-tube heat exchangers, *Appl. Therm. Eng*., 25 (2005) 1684-1696.
[20] Y. Chen, M. Fiebig and N. K. Mitra, Heat transfer enhancement of a finned oval tube with punched longitudinal vortex generators in-line, *Int. J. Heat Mass Transfer*, 41 (1998) 4151-4166.
[21] Y. Chen, M. Fiebig and N. K. Mitra, Heat transfer enhancement of finned oval tube with staggered punched longitudinal vortex generators, *Int. J. Heat Mass Transfer*, 43 (2000) 417-435.
[22] S. Tiwari, D. Maurya, G. Biswas and V. Eswaran, Heat transfer enhancement in cross-flow heat exchangers using oval tubes and multiple delta winglets, *Int. J. Heat Mass Transfer*, 46 (2003) 2841-2856.
[23] J. E. O'Brien, M. S. Sohal and P. C. Wallstedt, Local heat transfer and pressure drop for finned-tube heat exchangers using oval tubes and vortex generators, *J. Heat Transfer*, 126 (2004) 826-835.
[24] P. Chu, Y. L. He, Y. G. Lei, L. T. Tian and R. Li, Three-dimensional numerical study on fin-and-oval-tube heat exchanger with longitudinal vortex generators, *Appl. Therm. Eng*., 29 (2009) 859-876.
[25] A. I. ElSherbini and A. M. Jacobi, The thermal-hydraulic impact of delta-wing vortex generators on the performance of a plain-fin-and-tube heat exchanger, *HVAC&R Research,* 8 (4) (2002) 357-370.
[26] A. Joardar and A. M. Jacobi, Heat transfer enhancement by winglet-type vortex generator arrays in compact plain-fin-and-tube heat exchangers, *Int. J. Refrig*, 31 (2008) 87-97.
[27] A. Joardar and A. M. Jacobi, A numerical study of flow and heat transfer enhancement using an array of delta-winglet vortex generators in a fin-and-tube heat exchanger, *J. Heat Transfer*, 129 (9) (2006) 1156-1167.
[28] K. M. Kwak, K. Torii and K. Nishino, Heat transfer and flow characteristics of fin-tube bundles with and without winglet-type vortex generators, *Exp. in Fluids,* 33 (2002) 696-702.
[29] C. M. B. Russell, T. V. Jones and G. H. Lee, Heat transfer enhancement using vortex generators, *Heat Transfer, Proc. Seventh Heat Transfer Conference,* 3 (1982) 283-288.
[30] P. Sriromreun, C. Thianpong and P. Promvonge, Experimental and numerical study on heat transfer enhancement in a channel with Z-shaped baffles, *Int. Comm. Heat Mass Transfer*, 39 (2012) 945-952.

Withada Jedsadaratanachai has a doctorate in Mechanical Engineering, King Mongkut's Institute of Technology Ladkrabang (KMITL), Bangkok, Thailand. She is a lecturer in \ Mechanical Engineering, KMITL. Her research works are about computational fluid dynamic (CFD), mathematical model and thermo-fluid.

Amnart Boonloi is an Assistant Professor of Mechanical Engineering Technology at King Mongkut's University of Technology North Bangkok (KMUTNB), Thailand. He obtained his D.Eng. in Mechanical Engineering from King Mongkut's Institute of Technology Ladkrabang in 2011. His research interests include Thermal&Fluid engineering, heat transfer enhancement and computational fluid dynamics and drying technology.